Characterization of Divalent Metal Metavanadates by ^{51}V Magic-Angle Spinning NMR Spectroscopy of the Central and Satellite Transitions

Ulla Gro Nielsen, Hans J. Jakobsen,* and Jørgen Skibsted

Instrument Centre for Solid-State NMR Spectroscopy, Department of Chemistry, University of Aarhus, DK-8000 Aarhus C, Denmark

Received October 25, 1999

^{51}V quadrupole coupling and chemical shielding tensors have been determined from ^{51}V magic-angle spinning (MAS) NMR spectra at a magnetic field of 14.1 T for nine divalent metal metavanadates: $Mg(VO_3)_2$, $Ca(VO_3)_2$, $Ca(VO_3)_2{\cdot}4H_2O$, α-$Sr(VO_3)_2$, $Ba(VO_3)_2$, $Zn(VO_3)_2$, α- and β-$Cd(VO_3)_2$, and $Pb(VO_3)_2$. The manifold of spinning sidebands (ssbs) from the central and satellite transitions, observed in the ^{51}V MAS NMR spectra, have been analyzed using least-squares fitting and numerical error analysis. This has led to a precise determination of the eight NMR parameters characterizing the magnitudes and relative orientations of the quadrupole coupling and chemical shielding tensors. The optimized data show strong similarities between the NMR parameters for the isostructural groups of divalent metal metavanadates. This demonstrates that different types of metavanadates can easily be distinguished by their anisotropic NMR parameters. The brannerite type of divalent metal metavanadates exhibits very strong ^{51}V quadrupole couplings (i.e., $C_Q = 6.46-7.50$ MHz), which reflect the highly distorted octahedral environments for the V^{5+} ion in these phases. Linear correlations between the principal tensor elements for the ^{51}V quadrupole coupling tensors and electric field gradient tensor elements, estimated from point-monopole calculations, are reported for the divalent metal metavanadates. These correlations are used in the assignment of the NMR parameters for the different crystallographic ^{51}V sites of $Ca(VO_3)_2{\cdot}4H_2O$, $Pb(VO_3)_2$, and $Ba(VO_3)_2$. For α-$Sr(VO_3)_2$, with an unknown crystal structure, the ^{51}V NMR data strongly suggest that this metavanadate is isostructural with $Ba(VO_3)_2$, for which the crystal structure has been reported. Finally, the chemical shielding parameters for orthovanadates and mono- and divalent metal metavanadates are compared.

Introduction

Recent years have seen an increasing interest in the application of ^{51}V NMR spectroscopy to solid-state inorganic chemistry. Most attention has been paid to structural studies of vanadates with catalytic properties,[1−5] vanadium oxide-based catalysts,[1,2,6−16] and vanadium species in microporous framework structures.[16−21] This is partly due to the favorable properties of the ^{51}V isotope (99.8% natural abundance, $I = {}^7/_2$ with a small quadrupole moment and a relatively high gyromagnetic ratio) which allow observation of ^{51}V in very small quantities, such as those of vanadium incorporated into zeolite structures[16−21] and vanadium oxide on alumina or silica supports.[6−15] Furthermore, different vanadium species can be distinguished and characterized by a determination of the ^{51}V chemical shielding anisotropy (CSA) alone[1,2,5,9,22−24] or in combination with the quadrupole coupling parameters.[25−27] This makes the technique very useful in providing structural information about the local environments

* To whom correspondence should be addressed. Phone: +45-8942-3842. Fax: +45-8616-6199. E-mail: hja@kemi.aau.dk.

(1) Lapina, O. B.; Mastikhin, V. M.; Shubin, A. A.; Krasilnikov, V. N.; Zamaraev, K. I. *Prog. Nucl. Magn. Reson. Spectrosc*. **1992**, *24*, 457.
(2) Eckert, H.; Wachs, I. E. *J. Phys. Chem.* **1989**, *93*, 6796.
(3) Hardcastle, F. D.; Wachs, I. E.; Eckert, H.; Jefferson, D. A. *J. Solid State Chem.* **1991**, *90*, 194.
(4) Davis, J.; Tinet, D.; Fripiat, J. J.; Amarilla, J. M.; Casal, B.; Ruiz-Hitzky, E. *J. Mater. Res.* **1991**, *6*, 393.
(5) Crans, D. C.; Felty, R. A.; Chen, H.; Eckert, H.; Das, N. *Inorg. Chem.* **1994**, *33*, 2427.
(6) Taouk, B.; Guelton, M.; Grimblot, J.; Bonnelle, J. P. *J. Phys. Chem.* **1988**, *92*, 6700.
(7) Le Coustumer, L. R.; Taouk, B.; Le Meur, M.; Payen, E.; Guelton, M.; Grimblot, J. *J. Phys. Chem.* **1988**, *92*, 1230.
(8) Walther, K. L.; Kümmerlen, J.; Wokaun, A.; Baiker, A. *Ber. Bunsen-Ges. Phys. Chem.* **1993**, *97*, 772.
(9) Das, N.; Eckert, H.; Hu, H.; Wachs, I. E.; Walzer, J. F.; Feher, F. J. *J. Phys. Chem.* **1993**, *97*, 8240.
(10) Lapina, O. B.; Nosov, A. V.; Mastikhin, V. M.; Dubkov, K. A.; Mokrinski, V. V. *J. Mol. Catal.* **1994**, *87*, 57.
(11) Pinaeva, L. G.; Lapina, O. B.; Mastikhin, V. M.; Nosov, A. V.; Balshinimaev, B. S. *J. Mol. Catal.* **1994**, *88*, 311.
(12) Chary, K. V. R.; Kishan, G. *J. Phys. Chem.* **1995**, *99*, 14424.
(13) Mastikhin, V. M.; Terskikh, V. V.; Lapina, O. B.; Filimonova, S. V.; Seidl, M.; Knözinger, H. *Solid State Nucl. Magn. Reson.* **1995**, *4*, 369.
(14) Smits, R. H. H.; Seshan, K.; Ross, J. R. H.; Kentgens, A. P. M. *J. Phys. Chem.* **1995**, *99*, 9169.
(15) Sohn, J. R.; Cho, S. G.; Pae, Y. I.; Hayashi, S. *J. Catal.* **1996**, *159*, 170.
(16) Wang, C.-B.; Deo, G.; Wachs, I. E. *J. Catal.* **1998**, *178*, 640.
(17) Moudrakovski, I. L.; Sayari, A.; Ratcliffe, C. I.; Ripmeester, J. A.; Preston, K. F. *J. Phys. Chem.* **1994**, *98*, 10895.
(18) Blasco, T.; Concepción, P.; López Nieto, J. M.; Pérez-Pariente, J. *J. Catal.* **1995**, *152*, 1.
(19) Gontier, S.; Tuel, A. *Microporous Mater.* **1995**, *5*,161.
(20) Lakshmi, L. J.; Srinivas, S. T.; Rao, P. K.; Nosov, A. V.; Lapina, O. B.; Mastikhin, V. M. *Solid State Nucl. Magn. Reson.* **1995**, *4*, 59.
(21) Luan, Z.; Xu, J.; He, H.; Klinowski, J.; Kevan, L. *J. Phys. Chem.* **1996**, *100*, 19595.
(22) Hayashi, S.; Hayamizu, K. *Bull. Chem. Soc. Jpn.* **1990**, *63*, 961.
(23) Hayakawa, S.; Yoko, T.; Sakka, S. *Bull. Chem. Soc. Jpn.* **1993**, *66*, 3393.
(24) Hayakawa, S.; Yoko, T.; Sakka, S. *J. Solid State Chem.* **1994**, *112*, 329.
(25) Skibsted, J.; Nielsen, N. C.; Bildsøe, H.; Jakobsen, H. J. *J. Am. Chem. Soc.* **1993**, *115*, 7351.
(26) Skibsted, J.; Jacobsen, C. J. H.; Jakobsen, H. J. *Inorg. Chem.* **1998**, *37*, 3083.
(27) Skibsted, J.; Nielsen, N. C.; Bildsøe, H.; Jakobsen, H. J. *Chem. Phys. Lett.* **1992**, *188*, 405.

10.1021/ic991243z CCC: $19.00
Published on Web 04/14/2000

of vanadium species in systems with no long-range order, such as catalytic surfaces.

A fundamental aspect of ^{51}V NMR is the relationships between the NMR parameters, characterizing the chemical shielding (i.e., δ_σ, η_σ, and δ_{iso}) and the quadrupole coupling (C_Q and η_Q) interactions, and structural parameters, such as the state of coordination, the degree of polymerization of VO_n units, V−O−V/O−V−O bond angles, and V−O bond lengths. To establish these types of correlations, several ^{51}V NMR studies have focused on the characterization of crystalline, inorganic vanadates[1,2,22−26] with crystal structures known from X-ray diffraction. These investigations have mainly included ortho-, pyro-, and metavanadates and a determination of the ^{51}V CSA parameters from either static-powder or MAS NMR spectra of the ^{51}V central transition. Eckert and Wachs[2] have shown that the ^{51}V CSA generally increases with an increasing degree of polymerization for ortho-, pyro-, and metavanadates, while Hayakawa et al.[24] have suggested that the state of coordination and the degree of polymerization for VO_n polyhedra can be predicted from the CSA tensors.

In recent work, we showed that improved information about the ^{51}V environments can be obtained from a ^{51}V MAS NMR spectrum of all single-quantum transitions.[25−27] These experiments allow determination of the magnitudes and relative orientations of the ^{51}V CSA and quadrupole coupling tensors from numerical analysis of the spinning-sideband intensities observed in these spectra. In addition to the structural information gained from the quadrupole coupling parameters, a precise determination of the isotropic chemical shift (δ_{iso}) is also obtained. This is of importance when correlations between δ_{iso} and structural parameters are derived, since the second-order quadrupolar interaction may shift the isotropic peak by as much as 14 ppm to lower frequency at moderate magnetic fields (9.4 T). So far, ^{51}V MAS NMR spectroscopy of the central and satellite transitions has been employed in studies of orthovanadates and alkali metal metavanadates.[25,26] For these vanadates, correlations between the quadrupole couplings and estimated electric field gradient (EFG) tensors, obtained from point-charge calculations, have been reported. Furthermore, these studies show that simple relationships between the magnitudes of the CSA and the quadrupole couplings can only be expected for structurally closely related compounds, e.g., for the isostructural metavanadates MVO_3 (M = NH_4, K, Rb, Cs, Tl).[26]

This work reports the determination of the magnitudes and relative orientations of the ^{51}V quadrupole coupling and CSA tensors for a series of divalent metal metavanadates ($M(VO_3)_2$; M = Mg, Ca, Sr, Ba, Zn, Cd, Pb) using ^{51}V MAS NMR spectroscopy of the central and satellite transitions. These metavanadates are structurally quite different from those studied recently,[26] since they include vanadium coordinated to either four, five, or six oxygen atoms and in some cases contain multiple vanadium sites, which may complicate the analysis of the ^{51}V MAS NMR spectra. Thus, the ^{51}V NMR spectra are recorded at a high magnetic field (14.1 T) to improve the resolution of the individual resonances and to obtain an improved reflection of the effects from the CSA interaction.

^{51}V CSA parameters and chemical shifts have been reported earlier for divalent metal metavanadates from either ^{51}V static-powder or MAS NMR spectra of the central transition.[1,2,24] However, in some cases, resonances from structurally different vanadium sites (i.e., $M(VO_3)_2$; M = Sr, Ba, Pb) were not resolved, which led to inaccurate determinations of the ^{51}V CSA's and chemical shifts. The consideration of both interactions in this work is shown to significantly improve the precision of the ^{51}V CSA and quadrupole coupling parameters, thereby providing a more reliable basis for correlations of these data with structural parameters. The present work also includes an investigation of relationships between the ^{51}V quadrupole coupling parameters and structural data using point-charge calculations which model the electronic structure at the nuclear V^{5+} site.

Experimental Section

Materials. The vanadates studied were synthesized from reagents of analytical purity grade which were used without further purification. The basic structures and purities of the metavanadates were confirmed by powder X-ray diffraction using the JCPDS diffraction files as reference.

$Mg(VO_3)_2$. The preparation of $Mg(VO_3)_2$ was based on the method described by Sam et al.[28] A 5.27 g (45.0 mmol) amount of NH_4VO_3 was dissolved in 50 mL of a 1% NH_3 solution, and 1.31 g (22.5 mmol) of $Mg(OH)_2$ was added. The suspension was evaporated while being stirred, then dried at 110 °C for 2 days, and finally calcined at 700 °C for 24 h.

α- and β-$Cd(VO_3)_2$. β-$Cd(VO_3)_2$ was synthesized by heating equimolar amounts of CdO and V_2O_5 at 660 °C. After 30 h at this temperature, the sample was cooled to room temperature, which gave the high-temperature β form of $Cd(VO_3)_2$. The low-temperature form, α-$Cd(VO_3)_2$, was obtained from a solution of 1.96 g (12.9 mmol) of NH_4VO_3 and 1.51 g (6.45 mmol) of $Cd(NO_3)_2{\cdot}4H_2O$ in 100 mL of H_2O. The suspension was evaporated at 90 °C with stirring until the water was evaporated. The residue was subsequently dried at 120 °C for 2 days.

$Ca(VO_3)_2$ and $Ca(VO_3)_2{\cdot}4H_2O$. The synthesis of $Ca(VO_3)_2{\cdot}4H_2O$ followed the method described by Marvin et al.[29] A 0.57 g (5.5 mmol) amount of CaO was dissolved in 250 mL of water, and 1.82 g (10 mmol) of V_2O_5 was added with stirring. After 1 h, the solution had a pH about 6 but still contained residues of solid V_2O_5. Thus, 75 mL of a saturated $Ca(OH)_2$ solution was added, which raised the pH to about 7. The suspension was heated overnight at 70 °C and then filtered twice to remove the precipitate. The filtrate was slowly evaporated, and after 2 weeks, a yellow precipitate of $Ca(VO_3)_2{\cdot}4H_2O$ was filtered off. TGA analysis revealed that the dihydrate ($Ca(VO_3)_2{\cdot}2H_2O$) was formed at about 53 °C and the anhydrous metavanadate at about 117 °C. $Ca(VO_3)_2$ was obtained by heating $Ca(VO_3)_2{\cdot}4H_2O$ at 240 °C overnight.

$M(VO_3)_2$ (M = Sr, Ba, Zn, Pb). $Zn(VO_3)_2$ was prepared by heating equimolar amounts of ZnO and V_2O_5 at 600 °C for 24 h. After cooling, the product was ground and heated again to 600 °C for 24 h. α-$Sr(VO_3)_2$, $Ba(VO_3)_2$, and $Pb(VO_3)_2$ were synthesized by heating equimolar amounts of V_2O_5 and of $SrCO_3$, $BaCO_3$, and $PbCO_3$ at 620, 700, and 500 °C, respectively, for approximately 24 h.

NMR Measurements. Solid-state ^{51}V MAS NMR experiments were performed at 157.7 MHz (14.1 T) on a Varian INOVA-600 spectrometer using home-built CP/MAS probes for 4 and 5 mm o.d. rotors. In one case ($Mg(VO_3)_2$), a ^{51}V MAS NMR spectrum was recorded at 78.5 MHz on a Varian INOVA-300 spectrometer. Spinning speeds in the ranges 12−13 and 14−16 kHz were employed for the 5 and 4 mm Si_3N_4 rotors, respectively, and a stability of ±2 Hz was achieved using a Varian rotor-speed controller. The ^{51}V MAS NMR spectra were obtained by employing an exact magic-angle setting (adjusted using ^{23}Na MAS NMR of $NaNO_3$), spectral widths of 2 MHz, single-pulse excitation with a pulse width of 0.5−1.0 μs (for $\gamma H_1/2\pi \approx 70$ kHz), and a relaxation delay of 1 s. Baseline distortions were suppressed by a linear prediction of the first (10−25) data points of the FID followed by a baseline correction using the Varian VNMR software. Isotropic chemical shifts are reported relative to neat $VOCl_3$ using a solution of 0.16 M $NaVO_3$ ($\delta_{iso} = -574.38$ ppm) as a secondary reference.[25] However, the ^{51}V MAS NMR spectra shown in the figures employ a kHz scale relative to the isotropic peaks, to appreciate the asymmetry

(28) Sam, D. S. H.; Soenen, V.; Volta, J. C. *J. Catal.* **1990**, *123*, 417.
(29) Marvin, R.; Magin, G. B., Jr. *U.S. Geol. Surv. Prof. Pap.* **1959**, *320*, 103.

Table 1. ^{51}V Quadrupole Couplings (C_Q, η_Q), Chemical Shielding Anisotropies (δ_σ, η_σ), Relative Orientations of the Two Tensorial Interactions (ψ, χ, ξ), and Isotropic Chemical Shifts for a Series of Divalent Metal Metavanadates from ^{51}V MAS NMR at 14.1 T[a]

compd[b]		C_Q (MHz)	η_Q	δ_σ (ppm)	η_σ	ψ (deg)	χ (deg)	ξ (deg)	δ_{iso}[c] (ppm)
$Mg(VO_3)_2$		7.50 ± 0.10	0.34 ± 0.02	310 ± 3	0.30 ± 0.03	0[d]	52 ± 7	0 ± 17	−533.9 ± 0.5
$Zn(VO_3)_2$		6.86 ± 0.09	0.40 ± 0.02	333 ± 3	0.02 ± 0.06	0[d]	53 ± 6	2 ± 20	−493.8 ± 0.3
β-$Cd(VO_3)_2$		6.46 ± 0.09	0.47 ± 0.03	311 ± 3	0.31 ± 0.03	22 ± 36	55 ± 6	0 ± 18	−468.2 ± 0.3
α-$Cd(VO_3)_2$		1.70 ± 0.07	1.00 ± 0.10	484 ± 16	0.15 ± 0.09	0[d]	90 ± 4	47 ± 7	−521.5 ± 0.3
$Ca(VO_3)_2$		3.06 ± 0.06	0.51 ± 0.05	517 ± 5	0.18 ± 0.03	74 ± 36	86 ± 9	35 ± 3	−563.0 ± 0.5
$Ca(VO_3)_2 \cdot 4H_2O$	V(1)	4.18 ± 0.04	0.92 ± 0.03	297 ± 6	0.30 ± 0.03	150 ± 15	34 ± 8	54 ± 14	−580.0 ± 0.5
	V(2)	3.73 ± 0.05	0.57 ± 0.03	492 ± 5	0.16 ± 0.03	144 ± 18	50 ± 5	88 ± 16	−529.5 ± 0.5
$Pb(VO_3)_2$	V(1)	3.75 ± 0.05	0.13 ± 0.03	465 ± 5	0.15 ± 0.05	90 ± 55	36 ± 6	0[d]	−529.8 ± 0.3
	V(2)	6.98 ± 0.11	0.31 ± 0.02	428 ± 4	0.12 ± 0.05	90[d]	50 ± 5	0[d]	−479.7 ± 0.3
$Ba(VO_3)_2$	V(1)	3.68 ± 0.04	0.16 ± 0.02	190 ± 3	0.41 ± 0.08	153 ± 30	70 ± 7	60 ± 6	−658.5 ± 0.3
	V(2)	5.56 ± 0.04	0.04 ± 0.02	265 ± 3	0.59 ± 0.04	20 ± 20	8 ± 9[d]	90[d]	−590.6 ± 0.5
α-$Sr(VO_3)_2$	V(1)	4.22 ± 0.08	0.12 ± 0.04	218 ± 4	0.32 ± 0.10	128 ± 28	86 ± 23	43 ± 7	−639.1 ± 0.3
	V(2)	5.65 ± 0.14	0.31 ± 0.03	244 ± 4	0.61 ± 0.06	56 ± 36	6 ± 20	54 ± 39	−585.9 ± 0.3

[a] Optimized data from least-squares fits to the experimental ssb intensities observed in ^{51}V MAS NMR spectra at 14.1 T. The error estimates are based on calculations of the 95% confidence limits using the method described in ref 30. [b] Assignment of the ^{51}V parameters to the crystallographic ^{51}V sites employing the correlations between the quadrupole coupling tensor elements and estimates of the electric field gradient tensor elements from point-monopole calculations. The nonequivalent ^{51}V sites are indexed according to the structure references (cf. Table 2). [c] Isotropic chemical shift referenced to neat $VOCl_3$. [d] Parameters fixed in the optimization due to restrictions on the Euler angles imposed by the crystal symmetry (see text).

of the ssb manifolds, while insets displayed with a ppm scale are relative to neat $VOCl_3$.

Simulation Software. Simulations, least-squares fittings, and error analyses of the experimental ^{51}V MAS NMR spectra were performed on a SUN ULTRA-SPARC 1 workstation using the STARS solid-state NMR software package developed in our laboratory[25−27,30] and presently available as a part of the Varian VNMR software. The parameters for the magnitudes (C_Q, η_Q, δ_σ, and η_σ) and the relative orientation (the Euler angles ψ, χ, and ξ) of the two tensors were determined from least-squares fitting of simulated to experimental intensities of the spinning sidebands using the theoretical approach described elsewhere.[25,27] Effects from nonuniform detection (i.e., the quality factor (Q) of the probe circuitry[30]) have been included in the simulations, while distortions caused by nonuniform excitation are negligible, as justified elsewhere.[25,27] The error limits for the anisotropic NMR parameters are 95% confidence intervals calculated using the method described elsewhere.[30] The quadrupole coupling and CSA parameters are given by

$$C_Q = \frac{eQV_{zz}}{h} \qquad \eta_Q = \frac{V_{yy} - V_{xx}}{V_{zz}}$$

$$\delta_\sigma = \delta_{iso} - \delta_{zz} \qquad \eta_\sigma = \frac{\delta_{xx} - \delta_{yy}}{\delta_\sigma} \qquad (1)$$

where $\delta_{iso} = {}^1/_3(\delta_{xx} + \delta_{yy} + \delta_{zz})$. The principal tensor elements of the CSA ($\boldsymbol{\delta}$) and electric field gradient ($\mathbf{V}$) tensors are defined using the convention $|\lambda_{zz} - {}^1/_3\mathrm{Tr}(\lambda)| \geq |\lambda_{xx} - {}^1/_3\mathrm{Tr}(\lambda)| \geq |\lambda_{yy} - {}^1/_3\mathrm{Tr}(\lambda)|$ for $\lambda_{\alpha\alpha} = \delta_{\alpha\alpha}, V_{\alpha\alpha}$. The Euler angles ($\psi$, χ, ξ), describing the orientation of the CSA tensor relative to the quadrupole coupling tensor, correspond to positive rotations about δ_{zz} (ψ), the new δ_{yy} (χ), and the final δ_{zz} (ξ) axis. However, we note that the symmetry of the expressions for the first-order CSA and quadrupolar interactions and the averaging over all crystallite orientations implies that the ranges for the Euler angles can be reduced to $0 \leq \psi \leq \pi$ and $0 \leq \chi, \xi \leq \pi/2$ for powder NMR spectra.[25]

Results and Discussion

The determination of the ^{51}V CSA and quadrupole coupling parameters is described below for the individual samples of the divalent metal metavanadates. The optimized NMR parameters determined in this work are summarized in Table 1. Where possible, these parameters are compared with earlier reported data, and relationships between the ^{51}V point symmetries of the crystal structures and the ^{51}V NMR parameters are discussed. Finally, correlations between the NMR data and structural parameters derived from the reported crystal structures are investigated.

$Mg(VO_3)_2$. A series of divalent metal metavanadates have a structure which is very similar to the monoclinic structure of brannerite ($ThTi_2O_6$) with the space group $C2/m$.[31] These include $Mg(VO_3)_2$,[32] $Zn(VO_3)_2$,[33] and β-$Cd(VO_3)_2$,[34] which are studied in this work. For the brannerite type of metavanadates, the asymmetric unit includes a single vanadium atom located in a crystallographic mirror plane. Vanadium is coordinated to six oxygens in a distorted arrangement, which includes five V−O bonds with bond distances in the range 1.66−2.11 Å and a significant longer V−O bond, between 2.45 and 2.67 Å, for these metavanadates.

The ^{51}V MAS NMR spectrum (14.1 T, ν_r = 13.0 kHz) of the central and satellite transitions for $Mg(VO_3)_2$ is shown in Figure 1a. The most intense spinning sidebands (ssbs) in the center of the spectrum originate mainly from the central transition and reflect the contribution from a significant CSA, while the width of the ssb manifold, which exceeds the spectral width of 2 MHz, indicates a large quadrupole coupling. The expansions of two spectral regions (insets in Figure 1a) illustrate the observation of separate peaks from the individual transitions and the partly resolved second-order quadrupolar line shapes for the ssbs from the outer transitions ($m = \pm{}^5/_2$, $m = \pm{}^7/_2$). Similar splittings of the ssbs from the individual transitions were recently observed in the ^{51}V MAS NMR spectrum of the orthovanadate $BiVO_4$[26] and indicate a quite large quadrupole coupling for the ^{51}V site in $Mg(VO_3)_2$. Least-squares fitting of simulated to experimental ssb intensities for the spectrum in Figure 1a confirms this assumption, since C_Q = 7.50 MHz is obtained for $Mg(VO_3)_2$, which is one of the largest quadrupole couplings observed so far for ortho-, pyro-, and metavanadates. The optimization and error analysis do not allow a reliable determination of the Euler angle ψ. Thus, it is utilized that the V^{5+} ion in $Mg(VO_3)_2$ is situated in a mirror plane,[32] implying that one axis for each of the interaction tensors is perpendicular to this plane. This corresponds to two of the Euler angles being

(30) Skibsted, J.; Vosegaard, T.; Bildsøe, H.; Jakobsen, H. J. *J. Phys. Chem.* **1996**, *100*, 14872.
(31) Ruh, R.; Wadsley, A. D. *Acta Crystallogr.* **1966**, *21*, 974.
(32) Ng, H. N.; Calvo, C. *Can. J. Chem.* **1972**, *50*, 3619.
(33) Andreetti, G. D.; Calestani, G.; Montenero, A. *Z. Kristallogr.* **1984**, *168*, 53.
(34) Mocala, K.; Ziólkowski, J. *J. Solid State Chem.* **1987**, *69*, 299.

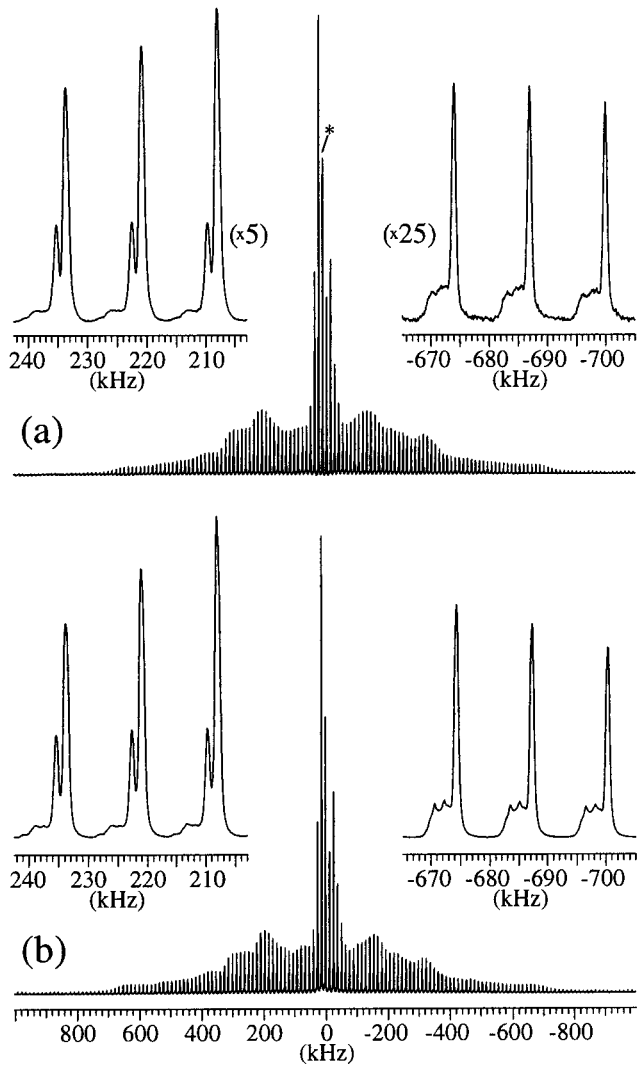

Figure 1. (a) Experimental ^{51}V MAS NMR spectrum of the central and satellite transitions for $Mg(VO_3)_2$ recorded at 14.1 T using ν_r = 13 kHz. (b) Simulated spectrum including the second-order quadrupolar broadening of the ssbs and employing the optimized parameters for $Mg(VO_3)_2$ in Table 1. A combination of 50 Hz Gaussian and 450 Hz Lorentzian line broadening was used for the ssbs in the simulation. The insets for two regions in (a) and (b) illustrate the splitting of the ssbs caused by the difference in second-order quadrupolar shift for the individual satellite transitions and the observation of partly resolved second-order quadrupolar line shapes for the outer ($m = \pm^5/_2$, $m = \pm^7/_2$) transitions (high-frequency side of the ssbs). The asterisk indicates the centerband.

constrained to values of $n \times 90°$ ($n = 0, 1, ...$). Using different combinations of the values for two of the Euler angles in five-parameter optimizations gives the lowest rms value for $\psi = \xi = 0°$, in agreement with the value for ξ obtained from seven-parameter fits. The optimum simulation, corresponding to the parameters for $Mg(VO_3)_2$ in Table 1 and including the second-order quadrupolar interaction, is illustrated in Figure 1b and is observed to convincingly reproduce the intensities and line shapes of the ssbs in the experimental spectrum (Figure 1a).

Figure 2 compares the regions for the central transitions in the ^{51}V MAS NMR spectra of $Mg(VO_3)_2$ recorded at 14.1 and 7.1 T using the same spinning speed. This comparison illustrates the direct and inverse proportionalities of the CSA and second-order quadrupolar interactions, respectively, with the magnetic field strength. The spectrum at high field (Figure 2a) gives an improved reflection of the CSA interaction and a significant reduction in line widths of the resonances compared to the 7.1-T

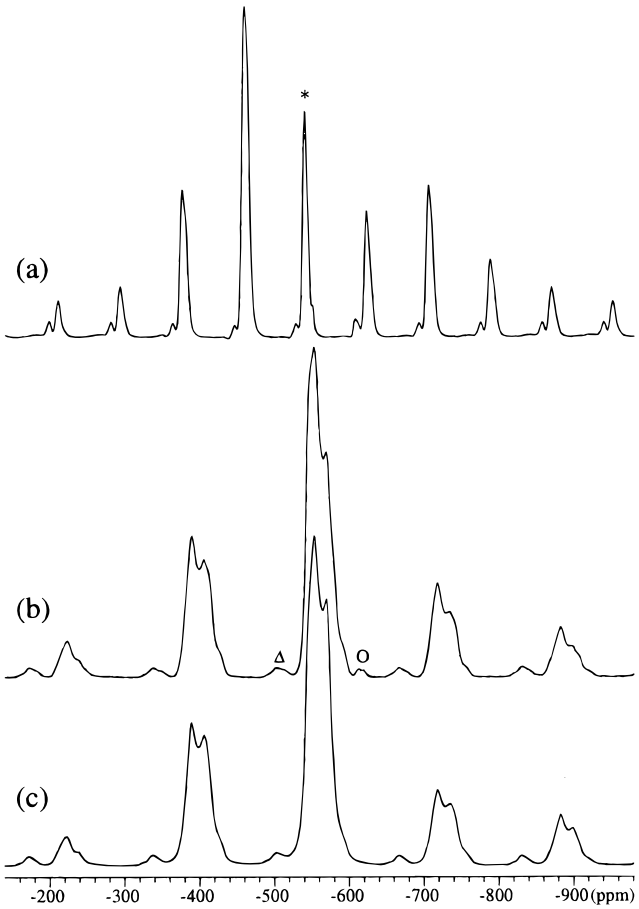

Figure 2. ^{51}V MAS NMR spectra (ν_r = 13 kHz) of $Mg(VO_3)_2$ recorded at (a) 14.1 T and (b) 7.1 T and illustrating the spectral region for the central transition. The asterisk in (a) indicates the isotropic peak, while the circle in (b) marks the centerband resonance from a minor impurity of $Mg_3(VO_4)_2$. The triangle in (b) indicates the centerband for the ($m = \pm^5/_2$, $m = \pm^3/_2$) transitions. (c) Simulation of the spectrum recorded at 7.1 T using the parameters in Table 1. The simulation includes the second-order quadrupolar interaction and a Lorentzian line broadning of 500 Hz for the ssbs.

spectrum (Figure 2b). Thus, NMR parameters of higher precision can be derived from numerical analysis of the high-field spectrum. In contrast, the 7.1-T spectrum exhibits well-resolved second-order line shapes of the ssbs from the central transition, allowing a determination of C_Q and η_Q from line shape simulations of the central transition only. An independent test of the reliability of the NMR parameters determined at 14.1 T (Table 1) was achieved from optimization to the complete manifold of ssbs from the central and satellite transitions at 7.1 T (not shown). This analysis resulted in NMR parameters in full agreement with those listed in Table 1 for $Mg(VO_3)_2$ and illustrated by the optimized simulation in Figure 2c.

^{51}V chemical shielding parameters for $Mg(VO_3)_2$ were reported earlier by Occelli et al. ($\delta_{iso} = -548$ ppm, $\delta_\sigma = 328$ ppm, and $\eta_\sigma = 0.28$),[35] Hayakawa et al. ($\delta_{iso} = -550$ ppm, $\delta_\sigma = 317$ ppm, and $\eta_\sigma = 0.25$),[24] and Lapina et al. ($\delta_{iso} = -576$ ppm, $\delta_\sigma = 374$ ppm, and $\eta_\sigma = 0.32$)[1] from ^{51}V static-powder or MAS NMR spectra of the central transition. The ^{51}V CSA parameters determined in this work agree favorably with those reported by Occelli et al.[35] and Hayakawa et al.[24] However, δ_{iso} deviates significantly from the value reported by Lapina et al.,[1] which may reflect the second-order quadrupolar shift of

(35) Occelli, M. L.; Maxwell, R. S.; Eckert, H. *J. Catal.* **1992**, *137*, 36.

the central transition not being considered by these authors. We note that the second-order quadrupolar interaction gives low-frequency shifts of the center of gravity for the central transition of 6.0 and 24.0 ppm at 14.1 and 7.1 T, respectively, for the ^{51}V site in $Mg(VO_3)_2$ (cf. Figure 2).

$Zn(VO_3)_2$. The ^{51}V MAS NMR spectrum of $Zn(VO_3)_2$ at 14.1 T (not shown) exhibits an ssb manifold from a single ^{51}V site which bears a close resemblance to the spectrum observed for $Mg(VO_3)_2$. However, separate peaks from the individual transitions are only partly resolved for $Zn(VO_3)_2$, indicating a somewhat smaller quadrupole coupling. Least-squares optimization for the ssb intensities observed for $Zn(VO_3)_2$ results in the optimized parameters given in Table 1 and in a simulated spectrum, which convincingly reproduces the experimental ssb intensities. The error analysis shows that the Euler angle ψ cannot be determined reliably from the experimental ssb intensities. This is ascribed to the fact that $\eta_\sigma \approx 0$, under which condition theory shows that ψ is undefined.[27] The ^{51}V chemical shielding parameters in Table 1 agree fairly with the data reported earlier for $Zn(VO_3)_2$ from ^{51}V static-powder and MAS NMR of the central transition.[2,23] However, our data should be of higher precision, taking into account that the present analysis also includes effects from the quadrupolar interaction.

***β*-$Cd(VO_3)_2$.** $Cd(VO_3)_2$ has two polymorphic forms of which the β form has the brannerite structure while α-$Cd(VO_3)_2$ is isostructural with $Ca(VO_3)_2$.[34,36−38] The ^{51}V MAS NMR spectrum of β-$Cd(VO_3)_2$ is shown in Figure 3a and reveals an ssb manifold with strong similarities to those observed for $Mg(VO_3)_2$ (Figure 1a) and $Zn(VO_3)_2$. Least-squares optimization to the ssb intensities in Figure 3a gives the ^{51}V parameters for β-$Cd(VO_3)_2$ in Table 1. The simulated spectrum shown in Figure 3b reproduces all spectral features observed in Figure 3a. ^{51}V chemical shielding data were reported earlier for β-$Cd(VO_3)_2$ by Lapina et al. ($\delta_{iso} = -500$ ppm, $\delta_\sigma = 330$ ppm, and $\eta_\sigma = 0.18$).[1] These data are in fair agreement with the CSA parameters in Table 1, while the reported value for δ_{iso} indicates that the second-order quadrupolar shift of the central transition was not considered. A comparison of the ^{51}V parameters for $Mg(VO_3)_2$, $Zn(VO_3)_2$, and β-$Cd(VO_3)_2$ (Table 1) shows that these metavanadates exhibit strong quadrupole couplings and strong similarities in the values for η_Q, δ_σ, and the χ angle. This indicates that $\eta_\sigma \approx 0.4$, $\delta_\sigma \approx 320$ ppm, and (ψ, χ, ξ) ≈ (0°, 53°, 0°) are characteristic ^{51}V values for the brannerite type of metavanadates. However, a large variation is observed for δ_{iso}, which ranges from −468 to −549 ppm for the three metavanadates.

Mocala and Ziólkowski investigated the two polymorphic forms of $Cd(VO_3)_2$ by DTA and high-temperature powder XRD and claimed that β-$Cd(VO_3)_2$ is the low-temperature form.[34] This is in disagreement with earlier studies of Bouloux et al.,[36] who reported the brannerite type of $Cd(VO_3)_2$ (i.e., the β form) to be the high-temperature form. We have performed several syntheses of $Cd(VO_3)_2$ and found that the β form is always formed when high temperatures ($T \geq 500$ °C) are used, while the formation of α-$Cd(VO_3)_2$ requires synthesis temperatures below approximately 150 °C. The strong similarities between the ^{51}V MAS spectrum of the high-temperature phase (Figure 3a) and those observed for $Mg(VO_3)_2$ and $Zn(VO_3)_2$ and between the low-temperature form and $Ca(VO_3)_2$ (cf. Figure 4) clearly reveal that β-$Cd(VO_3)_2$ is the high-temperature phase

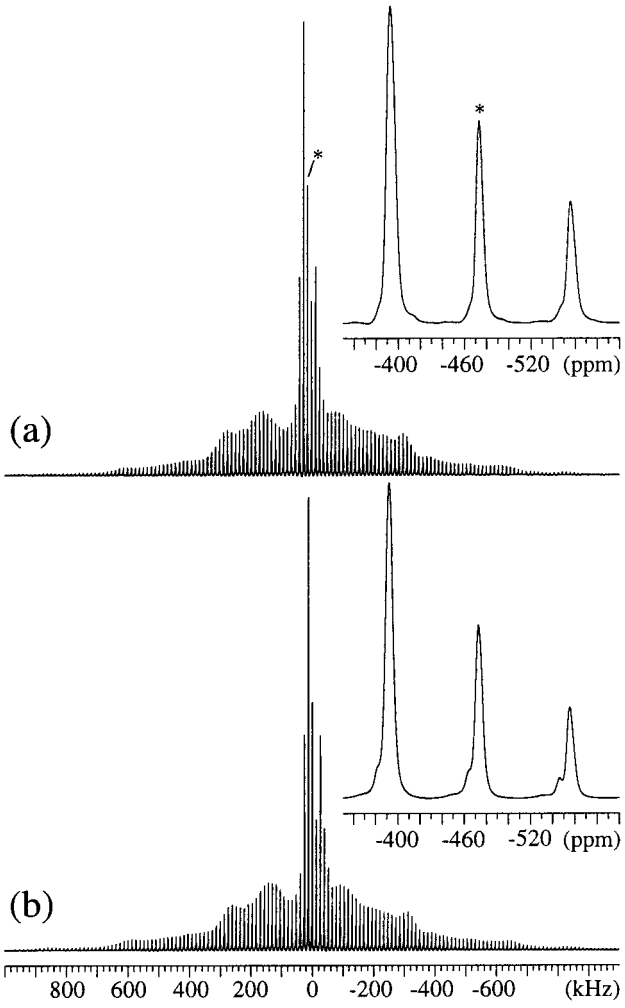

Figure 3. (a) Experimental ^{51}V MAS NMR spectrum of the central and satellite transitions for β-$Cd(VO_3)_2$ (14.1 T, $\nu_r = 13$ kHz). (b) Optimized simulation of the experimental spectrum using the parameters in Table 1. The insets in (a) and (b) illustrate the spectral region for the isotropic peak which is marked with an asterisk.

of the two polymorphic forms. This observation supports the findings of Bouloux et al.[36] but disagrees with the more recent study of Mocala and Ziólkowski.[34]

α-$Cd(VO_3)_2$ and $Ca(VO_3)_2$. Although α-$Cd(VO_3)_2$ and $Ca(VO_3)_2$ also crystallize in the monoclinic space group *C*2/*m*,[36−38] the structure of these two metavanadates deviates from the brannerite structure in that only five V−O contacts exist within a 3-Å distance, which results in a trigonal bipyramidal coordination for the V^{5+} ions. The ^{51}V MAS NMR spectra of α-$Cd(VO_3)_2$ and $Ca(VO_3)_2$ are shown in parts a and c, respectively, of Figure 4 and illustrate quite similar ssb manifolds for the two isostructural metavanadates. However, a comparison of these manifolds with those observed for the brannerite type of metavanadates (Figures 1 and 3) reveals that α-$Cd(VO_3)_2$ and $Ca(VO_3)_2$ possess smaller quadrupolar couplings and larger CSA's than the brannerite type of metavanadates. Thus, the two types of metavanadates can easily be distinguished by ^{51}V MAS NMR. Least-squares fittings to the experimental ssb manifolds in Figure 4a,c give the ^{51}V parameters for α-$Cd(VO_3)_2$ and $Ca(VO_3)_2$ in Table 1 and the optimized simulation for α-$Cd(VO_3)_2$ illustrated in Figure 4b. Within the error limits, the Euler angles ψ and χ are 90° for both metavanadates, in accord with the location of the V^{5+} ion in a mirror plane. The CSA parameters

(36) Bouloux, J.-C.; Perez, G.; Galy, J. *Bull. Soc. Fr. Mineral. Cristallogr.* **1972**, *95*, 130.
(37) Perez, G.; Frit, B.; Bouloux, J.-C.; Galy, J. *C. R. Seances Acad. Sci., Ser. C* **1970**, *270*, 952.
(38) Garnier, G.; Weigel, D. *J. Solid State Chem.* **1983**, *47*, 16.

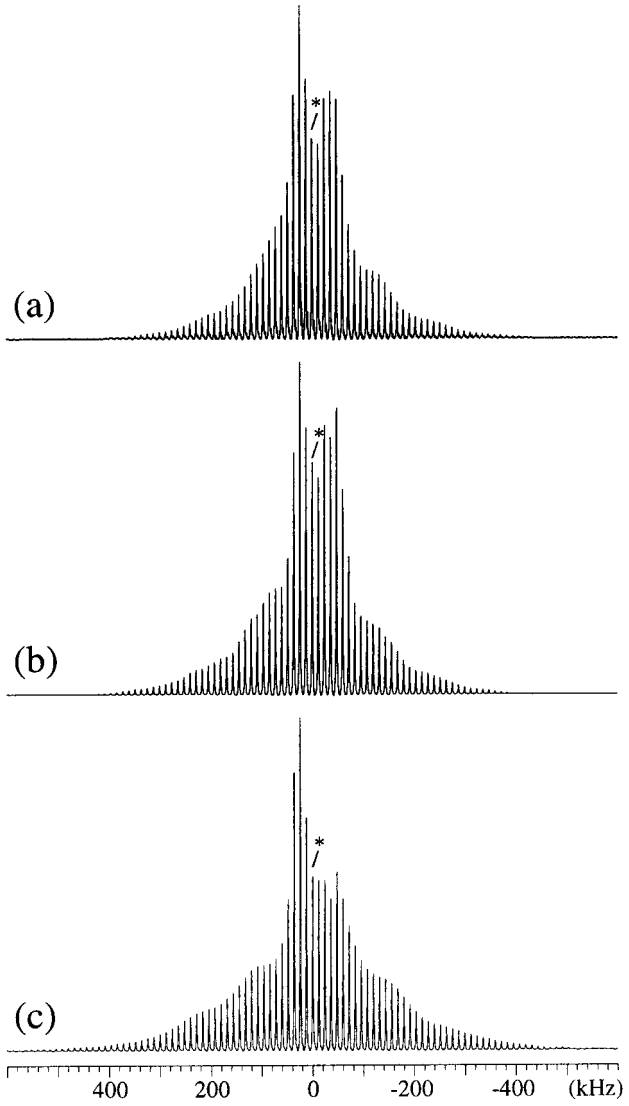

Figure 4. Experimental ^{51}V MAS NMR spectra of (a) α-$Cd(VO_3)_2$ and (c) $Ca(VO_3)_2$ recorded at 14.1 T using $\nu_r = 12$ kHz. (b) Simulated ^{51}V MAS NMR spectrum of α-$Cd(VO_3)_2$ using the parameters in Table 1 and a Gaussian line broadening of 1600 Hz for the ssbs. The isotropic peaks are marked by asterisks.

for $Ca(VO_3)_2$ in Table 1 are in good agreement with those reported earlier in the literature from ^{51}V static-powder and MAS NMR of the central transition,[1,24] while some discrepancies are observed for δ_{iso}, probably due to the fact that the second-order quadrupolar shift of the central transition has not been considered in these studies.

$Ca(VO_3)_2 \cdot 4H_2O$. Calcium metavanadate tetrahydrate, which occurs in nature as the mineral rossite, belongs to the triclinic space group $P\bar{1}$.[39] The structure includes two different vanadium atoms in the asymmetric unit which are coordinated to five oxygens in trigonal bipyramidal arrangements. The ^{51}V MAS NMR spectrum of $Ca(VO_3)_2 \cdot 4H_2O$, shown in Figure 5a, exhibits two overlapping manifolds of ssbs. The individual ssbs are well separated, due to a difference in chemical shift of about 50 ppm for the two sets of resonances. Least-squares fitting of simulated to experimental ssb intensities for the two manifolds gives the ^{51}V parameters in Table 1 for the two ^{51}V sites in $Ca(VO_3)_2 \cdot 4H_2O$. The optimized simulation of the total spectrum is shown in Figure 5b, while parts c and d of Figure 5 illustrate separate simulations of the ssb manifolds for the two different ^{51}V sites. The observation of Euler angles that deviate from 0° modulo 90° is in accord with the triclinic crystal structure for $Ca(VO_3)_2 \cdot 4H_2O$. Both sites possess similar quadrupolar couplings, while the V(2) site has a significantly larger shielding anisotropy (δ_σ) compared to that of the V(1) site. The CSA parameters for the V(2) site are quite similar to those observed for $Ca(VO_3)_2$.

$Pb(VO_3)_2$. Lead metavanadate crystallizes in the orthorhombic space group *Pnma*[40] and includes two unique V^{5+} ions, both situated on mirror planes. Each V^{5+} ion has five V−O bonds with bond distances in the range 1.61−2.06 Å and a sixth V−O contact with bond lengths of 2.57 and 2.73 Å for the two ^{51}V sites.[40] The ^{51}V MAS NMR spectrum of the central and satellite transitions for $Pb(VO_3)_2$, shown in Figure 6a, exhibits two overlapping ssb manifolds for which the individual ssbs are well separated at 14.1 T using a spinning speed of 13 kHz. The expansion of the region for the central transitions (Figure 6a) displays two additional resonances with low intensities at about −516 and −520 ppm, which originate from a minor impurity in the sample. Powder XRD reveals that the sample contains a small amount of $Pb_2V_2O_7$, and thus, the two resonances at −516 and −520 ppm are assigned to the isotropic peaks for the two unique ^{51}V sites in $Pb_2V_2O_7$.[41] Figure 6b displays the optimized simulation of the ssb intensities for the two ^{51}V sites in $Pb(VO_3)_2$ and corresponds to the parameters listed in Table 1 for this phase. The optimizations and error analyses show that reliable values of ψ for one of the sites and of ξ for both sites cannot be obtained from the experimental ssb intensities. Thus, we utilize that both V^{5+} ions are situated on mirror planes which constrain two of the Euler angles to values of 0° modulo 90°. The lowest rms deviation between simulated and experimental ssb intensities is obtained for $\psi = 90°$ and $\xi = 0°$ for both sites. From the NMR parameters in Table 1, it is apparent that the two ^{51}V sites in $Pb(VO_3)_2$ possess quite different quadrupole couplings but very similar CSA's. ^{51}V chemical shielding parameters for $Pb(VO_3)_2$ were reported earlier from ^{51}V static-powder and MAS NMR spectra of the central transition by Eckert and Wachs[2] ($\delta_\sigma = 467$ ppm, $\eta_\sigma = 0.02$, $\delta_{iso} = -533$ ppm) and Hayakawa et al.[24] ($\delta_\sigma = 450$ ppm, $\eta_\sigma = 0.16$, $\delta_{iso} = -532$ ppm), however, in both studies, only for one ^{51}V resonance. Hayakawa et al. observed only one manifold of ssbs from the central transition at 9.4 T for $\nu_r = 4-6$ kHz and ascribed this observation to a strong similarity in ^{51}V environments for the two sites in $Pb(VO_3)_2$.[24] The lack of resolution probably reflects the use of a too low spinning speed, since we have observed that a complete resolution of the ssb manifolds from the two sites at 9.4 T is only achieved for spinning speeds above 10 kHz.

$Ba(VO_3)_2$. The single-crystal XRD study of $Ba(VO_3)_2$ shows that this metavanadate crystallizes in the orthorhombic space group $C222$.[42] $Ba(VO_3)_2$ differs from most other divalent metavanadates since its structure includes chains of VO_4 tetrahedra similar to those found in the alkali metal metavanadates. The chains of VO_4 tetrahedra include two different V^{5+} ions, of which one is situated on a 2-fold axis, implying that the two sites, V(1) and V(2), have the ratio 2:1, respectively.[42] The ^{51}V MAS NMR spectrum of $Ba(VO_3)_2$, shown in Figure 7a, displays two overlapping ssb manifolds corresponding to a large and somewhat smaller quadrupole coupling. Examination of the relative intensities for the two ssb manifolds shows that the manifold exhibiting the large quadrupole coupling has the

(39) Ahmed, F. R.; Barnes, W. H. *Can. Mineral.* **1963**, *7*, 713.
(40) Jordan, B. D.; Calvo, C. *Can. J. Chem.* **1974**, *52*, 2701.
(41) Shannon, R. D.; Calvo, C. *Can. J. Chem.* **1973**, *51*, 70.
(42) Yao, T.; Oka, Y.; Yamamoto, N. *Inorg. Chim. Acta* **1995**, *238*, 165.

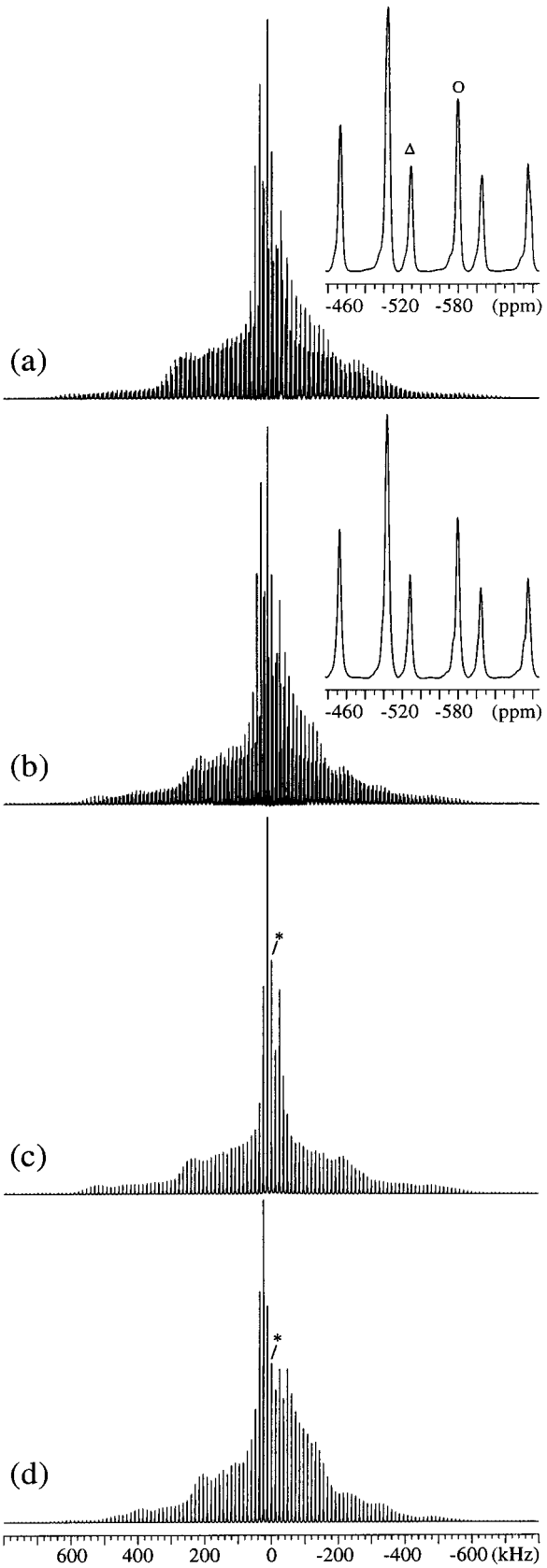

Figure 5. (a) Experimental and (b) simulated ^{51}V MAS NMR spectra of $Ca(VO_3)_2 \cdot 4H_2O$ (14.1 T, $\nu_r = 12$ kHz). The insets in (a) and (b) show the spectral region for the isotropic peaks which are indicated by a circle and a triangle for V(1) and V(2), respectively. The simulation employed the optimized ^{51}V NMR parameters for V(1) and V(2) in Table 1 and an intensity ratio of 1:1 for the two ssb manifolds. Parts c and d illustrate separate simulations of the ssb manifolds for V(1) and V(2), respectively.

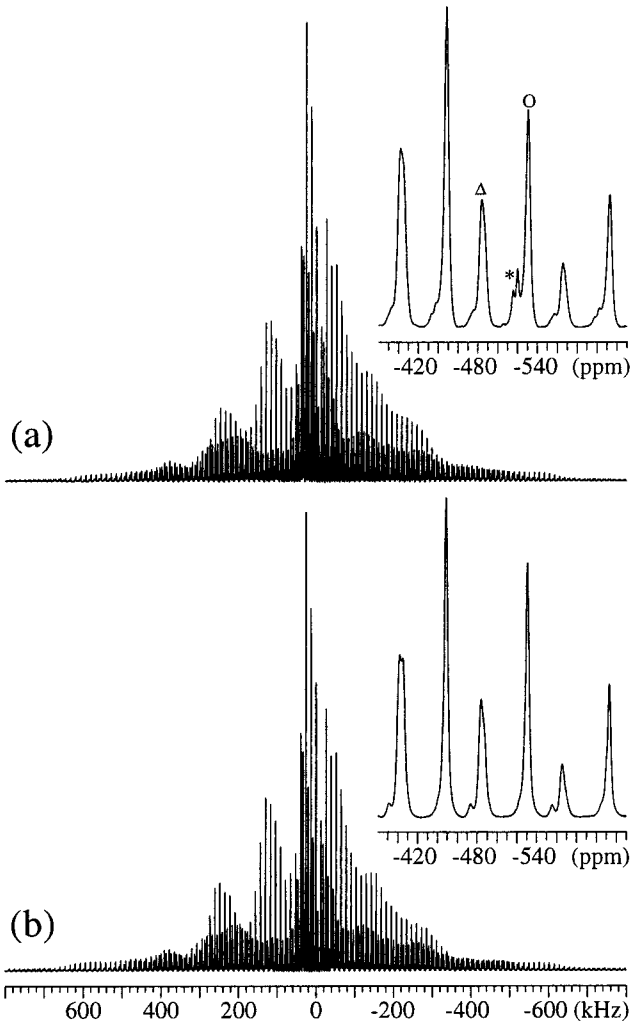

Figure 6. (a) Experimental and (b) simulated ^{51}V MAS NMR spectra of $Pb(VO_3)_2$ (14.1 T, $\nu_r = 13$ kHz). The simulation employed the optimized parameters for the V(1) and V(2) sites of $Pb(VO_3)_2$ in Table 1, 450 Hz Lorentzian and 100 Hz Gaussian line broadnings for the ssbs, and a 1:1 intensity ratio for the two ssb manifolds. The insets illustrate the spectral region for the isotropic peaks which are indicated by a circle and a triangle for V(1) and V(2), respectively. The isotropic peaks from a small impurity of $Pb_2V_2O_7$ are indicated by an asterisk in the inset for the experimental spectrum.

lowest intensity. Thus, this manifold is assigned to the V(2) site, which is situated on a 2-fold axis. The initial optimization and error analysis for the V(2) site give the Euler angles (ψ, χ, ξ) = (20 ± 20°, 8 ± 9°, 90°). These data fulfill the constraints imposed by the crystal symmetry for $\chi = 0°$ and $\xi = 90°$. Therefore, $\chi = 0°$ and $\xi = 90°$ are subsequently used as fixed parameters in five-parameter fits of the ssb intensities for V(2), resulting in the final parameters listed in Table 1. The optimized simulation is illustrated in Figure 7b and employs an intensity ratio of 0.75:1 for the V(2) and V(1) sites, respectively. This intensity ratio gives the best agreement between the experimental and simulated spectra, although a 1:2 ratio is expected for the two ssb manifolds from the XRD results.[42]

α-Sr(VO$_3$)$_2$. Strontium metavanadate has two polymorphic forms, of which the low-temperature phase, α-$Sr(VO_3)_2$, crystallizes in one of the orthorhombic space groups *C*222, *Cmm*2, and *Cmmm* according to a powder XRD investigation.[43] The

(43) Bouloux, J.-C.; Galy, J.; Hagenmuller, P. *Rev. Chim. Miner.* **1974**, *11*, 48.

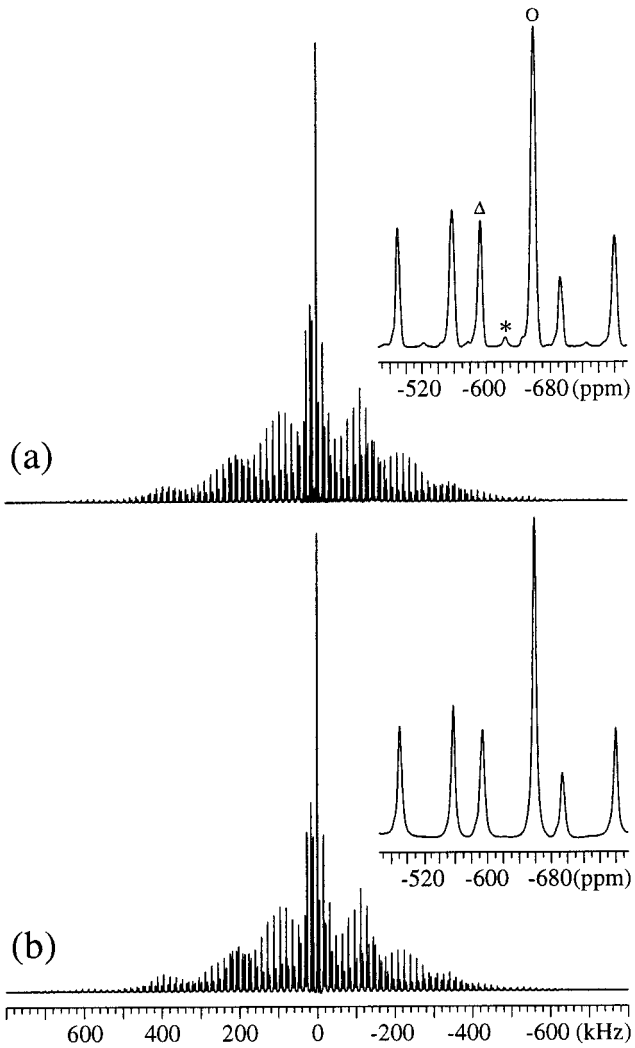

Figure 7. (a) Experimental and (b) simulated ^{51}V MAS NMR spectra of $Ba(VO_3)_2$ (14.1 T, $\nu_r = 16$ kHz). The parameters for V(1) and V(2) of $Ba(VO_3)_2$ in Table 1, a relative intensity ratio of 1:0.75 for V(1) and V(2), and a 700 Hz Gaussian line broadning were used for the simulated spectrum. The insets illustrate the spectral region for the isotropic peaks which are marked with a circle and a triangle for V(1) and V(2), respectively. The isotropic peak from a small impurity of $Ba_3(VO_4)_2$ is indicated by an asterisk.

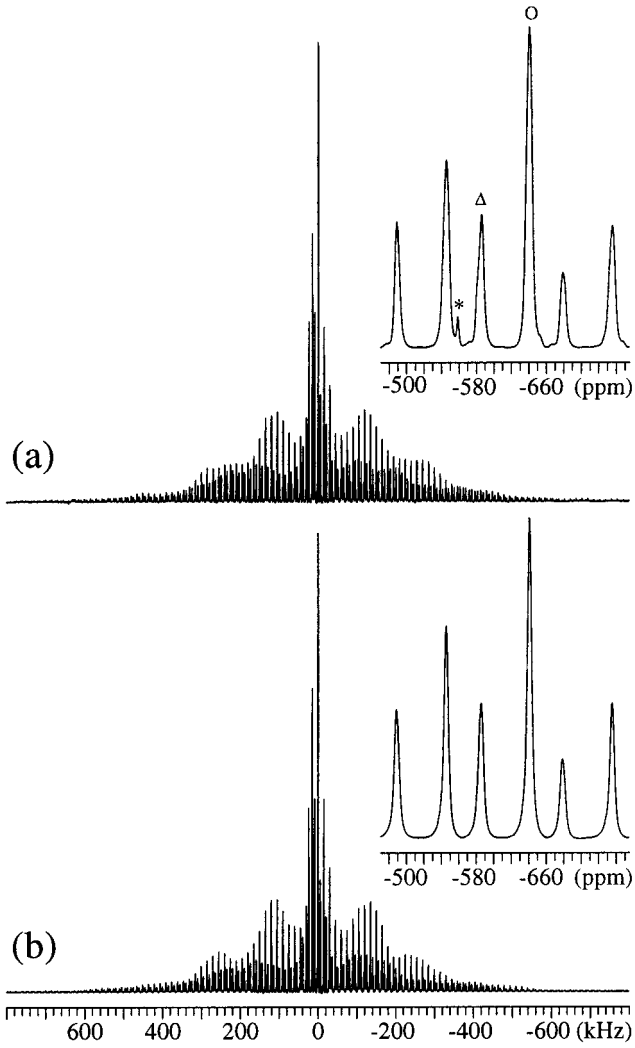

Figure 8. (a) Experimental ^{51}V MAS NMR spectrum of the central and satellite transitions for α-$Sr(VO_3)_2$ (14.1 T, $\nu_r = 15$ kHz). (b) Optimized simulation using the parameters for V(1) and V(2) of α-$Sr(VO_3)_2$ in Table 1. The simulation employed 650 Hz Lorentzian and 300 Hz Gaussian line broadnings for the ssbs and a relative intensity ratio of 1:0.67 for the V(1) and V(2) ssb manifolds, respectively. The insets illustrate the spectral region for the isotropic peaks which are indicated by a circle (V(1)) and a triangle (V(2)). The centerband from a small impurity of β-$Sr_2V_2O_7$ is indicated by an asterisk.

detailed structure of α-$Sr(VO_3)_2$ is not known; however, it is expected to resemble the structure of $Ba(VO_3)_2$. The ^{51}V MAS NMR spectrum of α-$Sr(VO_3)_2$, shown in Figure 8a, exhibits ssb manifolds from two distinct ^{51}V sites. Least-squares optimization to these manifolds gives the parameters for α-$Sr(VO_3)_2$ in Table 1 and the optimized simulation illustrated in Figure 8b. The best agreement between experimental and simulated ssb intensities is obtained using an intensity ratio of 0.67:1 for the two ^{51}V sites in the simulation. This ratio is similar to the intensity ratio for V(2) and V(1) in the simulation of the ^{51}V MAS spectrum for $Ba(VO_3)_2$. Furthermore, comparison of the NMR parameters for these two metavanadates shows close similarities in C_Q, δ_σ, η_σ, χ, and δ_{iso} for the V(1) and V(2) sites of α-$Sr(VO_3)_2$ and $Ba(VO_3)_2$. This indicates the presence of very similar symmetries and geometries for the VO_4 units in α-$Sr(VO_3)_2$ and $Ba(VO_3)_2$, which strongly suggest that these two metavanadates are isostructural compounds (i.e., space group *C*222). Hayakawa et al.[24] reported the chemical shielding parameters ($\delta_\sigma = 189$ ppm, $\eta_\sigma = 0.29$, and $\delta_{iso} = -644$ ppm) for α-$Sr(VO_3)_2$, determined from a ^{51}V MAS spectrum (9.4 T) of the central transition that only displayed a single set of ssbs. These data agree fairly well with those in Table 1 for the V(1) site of α-$Sr(VO_3)_2$, which has a 2-fold larger occupancy compared to V(2). Thus, the resonance from V(1) is expected to dominate the ^{51}V NMR spectrum in cases where the two ssb manifolds cannot be resolved.

Relationships between the ^{51}V NMR Parameters and Crystal Structure data. In our recent ^{51}V MAS NMR study of ortho- and metavanadates,[26] linear correlations between the experimental quadrupole coupling tensor elements (Q_{ii}^{exp}) and estimated values for the electric field gradient (EFG) tensor elements (V_{ii}^{est}) were observed for these types of vanadates. The estimated EFG tensor elements were obtained from point-monopole calculations,[44] which only consider the oxygen anions within the first coordination sphere of the V^{5+} ion and employ effective charges (q_i) for the oxygen anions. The effective oxygen charges are obtained as $q_i = (-2 + \sum f_{ij})e$, where f_{ij} is the covalence of the oxygen (i)−cation (j) bond, calculated from the equations of Brown and Shannon[45] and from the chemical

(44) Cohen, M. H.; Reif, F. *Solid State Phys.* **1957**, *5*, 321.

Table 2. Estimated Principal Elements (V_{ii}^{est}) (10^{20} V m^{-2}) of the ^{51}V Electric Field Gradient Tensor for the Series of Divalent Metal Metavanadates[a]

compd		V_{xx}^{est}	V_{yy}^{est}	V_{zz}^{est}	struct ref[b]
$Mg(VO_3)_2$		−1.638	−0.237	1.875	32
$Zn(VO_3)_2$		−1.629	−0.512	2.141	33
β-$Cd(VO_3)_2$		−1.878	−1.014	2.892	34
α-$Cd(VO_3)_2$		−0.590	−0.109	0.699	36
$Ca(VO_3)_2$		−0.986	−0.528	1.514	37
$Ca(VO_3)_2{\cdot}4H_2O$	V(1)	−1.269	−0.401	1.670	39
	V(2)	−1.094	−0.323	1.417	
$Pb(VO_3)_2$	V(1)	−2.188	−0.098	2.286	40
	V(2)	−1.980	−0.732	2.712	
$Ba(VO_3)_2$	V(1)	−1.212	−0.209	1.421	42
	V(2)	−1.705	−0.754	2.459	
α-$Sr(VO_3)_2$	V(1)	−1.593	−0.103	1.696	42, 43
	V(2)	−1.775	−0.720	2.495	

[a] Estimated values from point-monopole calculations using effective charges for the oxygen atoms surrounding the vanadium ion. The calculations employed tetrahedral coordination for the V^{5+} ions in $Ba(VO_3)_2$ and α-$Sr(VO_3)_2$, while pentacoordination was assumed for the remaining metavanadates (see text). [b] References for the structures reported from X-ray diffraction.

bond data of Brown and Altermatt.[46] Similar correlations have been reported for ^{23}Na in a series of sodium compounds[47] and for ^{133}Cs in inorganic cesium salts.[30]

To investigate the applicability of this approach for divalent metal metavanadates and to assign the observed ^{51}V NMR parameters to the individual crystallographic sites for $Ca(VO_3)_2{\cdot}4H_2O$, $Pb(VO_3)_2$, and $Ba(VO_3)_2$, estimated ^{51}V EFG tensor elements are calculated by employing the structural data reported from single-crystal XRD. Obviously, the experimental (Q_{ii}^{exp}) and calculated (V_{ii}^{est}) tensor elements can only be correlated for V^{5+} ions in the same coordination state, since our approach only considers the oxygen anions within the first coordination sphere of the ^{51}V site. Thus, we consider the ^{51}V sites in the brannerite type of metavanadates and in $Pb(VO_3)_2$ as VO_5 units, which allows us to compare the data for these vanadates with those for α-$Cd(VO_3)_2$, $Ca(VO_3)_2$, and $Ca(VO_3)_2{\cdot}4H_2O$. This is an acceptable approximation, since the V^{5+} ions in the brannerite type of metavanadates and in $Pb(VO_3)_2$ contain one long and five short V−O contacts. For $Ca(VO_3)_2{\cdot}4H_2O$, contributions to the oxygen bond valences from hydrogen bonds are calculated from the oxygen−oxygen (O···H−O) distances, using the relationship between the bond valence for H···O and the O···H−O distance in Figure 2 of ref 46, since the atomic coordinates for the H atoms were not determined in the single-crystal XRD study.[39] The effective oxygen charges range from −0.55*e* (O(2) for α-$Sr(VO_3)_2$) to −1.23*e* (O(1) for $Pb(VO_3)_2$) for the divalent metal metavanadates. The calculated V_{ii}^{est} elements are summarized in Table 2 and correlated with the corresponding Q_{ii}^{exp} elements in Figure 9a for the metavanadates containing VO_5 units. The Q_{ii}^{exp} elements are derived from C_Q and η_Q according to

$$Q_{zz}^{exp} = C_Q, \qquad Q_{yy}^{exp} = -{}^1/_2(1-\eta_Q)C_Q, \qquad Q_{xx}^{exp} = -{}^1/_2(1+\eta_Q)C_Q \quad (2)$$

assuming a positive value for C_Q. A linear relationship between the Q_{ii}^{exp} and V_{ii}^{est} elements is observed in Figure 9a, where linear regression analysis of the data gives the equation

$$Q_{ii}^{exp}\,(\mathrm{MHz}) = 2.45 V_{ii}^{est}\,(10^{20}\ \mathrm{V\ m^{-2}}) \quad (3)$$

with a correlation coefficient $R = 0.95$. This relationship is used in the tentative assignment (given in Table 2) of the observed NMR parameters for the crystallographic V(1) and V(2) sites of $Ca(VO_3)_2{\cdot}4H_2O$ and $Pb(VO_3)_2$. The plot of Q_{ii}^{exp} as function of V_{ii}^{est} in Figure 9a shows a somewhat larger scattering compared to the correlations reported for orthovanadates and monovalent metal metavanadates.[26] The larger scattering may

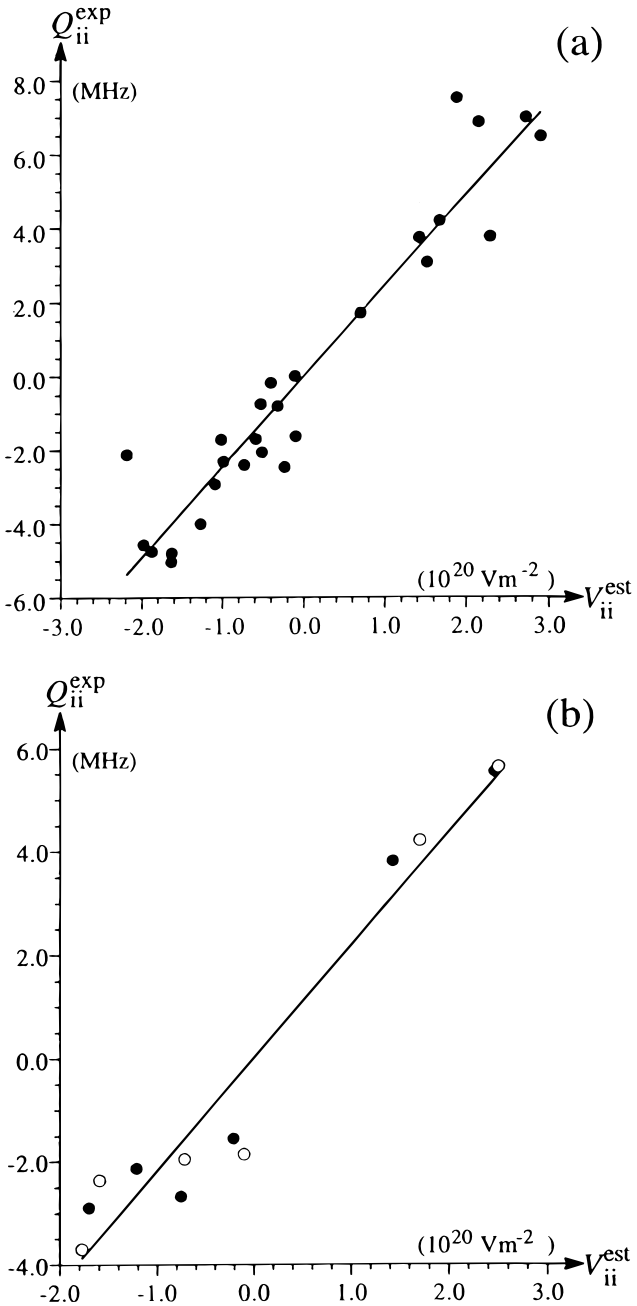

Figure 9. Linear correlations between ^{51}V quadrupole coupling tensor elements (Q_{ii}^{exp}) and estimated EFG tensor elements (V_{ii}^{est}) from point-monopole calculations for divalent metal metavanadates including (a) VO_5 or VO_6 units (see text) and (b) VO_4 tetrahedra ($Ba(VO_3)_2$, filled circles; α-$Sr(VO_3)_2$, open circles). The calculated values for V_{ii}^{est} are summarized in Table 2, while the results from linear regression analysis of the data in (a) and (b) are given in eqs 3 and 4, respectively.

(45) Brown, I. D.; Shannon, R. D. *Acta Crystallogr., Sect. A* **1973**, *29*, 266.
(46) Brown, I. D.; Altermatt, D. *Acta Crystallogr., Sect. B* **1985**, *41*, 244.
(47) Koller, H.; Engelhardt, G.; Kentgens, A. P. M.; Sauer, J. *J. Phys. Chem.* **1994**, *98*, 1544.

reflect the approximation of the ^{51}V coordination spheres for the brannerite type of metavanadates and $Pb(VO_3)_2$ to a VO_5 unit or that some of the XRD structures are of low precision, taking into account that most of these data were reported about three decades ago.

An assignment of the NMR parameters observed for the two ^{51}V sites in $Ba(VO_3)_2$ and α-$Sr(VO_3)_2$ to the crystallographic V(1) and V(2) sites is obtained from similar calculations for the VO_4 units in these vanadates. For α-$Sr(VO_3)_2$, it is assumed that this phase is isostructural with $Ba(VO_3)_2$ (vide supra). Thus, we employ the unit cell parameters for α-$Sr(VO_3)_2$ reported from powder XRD[43] but the fractional coordinates for $Ba(VO_3)_2$ in the calculations of the V_{ii}^{est} elements. These elements and the tentative assignment of the NMR parameters are included in Table 2, while Figure 9b illustrates a plot of Q_{ii}^{exp} as function of V_{ii}^{est} for $Ba(VO_3)_2$ and α-$Sr(VO_3)_2$. Linear regression analysis of the tensor elements for $Ba(VO_3)_2$ and α-$Sr(VO_3)_2$ gives the equation

$$Q_{ii}^{exp}\,(\mathrm{MHz}) = 2.21 V_{ii}^{est}\,(10^{20}\ \mathrm{V\ m^{-2}}) - 0.02 \qquad (4)$$

and the correlation coefficient $R = 0.97$. The slope in eq 4 is very similar to those reported for the orthovanadates and monovalent metavanadates.[26] This indicates that the relationship between Q_{ii}^{exp} and V_{ii}^{est} in eq 4 is also valid for other types of vanadates which contain VO_4 units. Furthermore, the good correlation between the Q_{ii}^{exp} and V_{ii}^{est} elements for α-$Sr(VO_3)_2$ supports the indication of this vanadate being isostructural with $Ba(VO_3)_2$ (vide supra).

Although similarities in the CSA parameters and Euler angles (ψ, χ, ξ) have been observed for the isostructural groups of divalent metal metavanadates, relationships between the CSA data and structural parameters appear less straightforward as compared to those for the quadrupole coupling parameters. Figure 10 compares the CSA parameters for orthovanadates, monovalent metal metavandates, and the divalent metal metavanadates studied in this work by illustrating the CSA asymmetry parameter (η_σ) as a function of the shielding anisotropy (δ_σ). It is apparent from this plot that the three types of vanadates can be distinguished on the basis of the CSA parameters. The orthovanadates possess the smallest shielding anisotropy (i.e., $\delta_\sigma \leq 100$ ppm) and the monovalent metal metavanadates exhibit characteristic asymmetry parameters of $\eta_\sigma = 0.71 \pm 0.05$, in agreement with earlier findings.[2,24,26] The divalent metal metavanadates including VO_5 or VO_6 units possess the largest δ_σ values and η_σ values below 0.3, while the CSA parameters for α-$Sr(VO_3)_2$ and $Ba(VO_3)_2$ are observed between the values for the monovalent metal metavanadates and the divalent metal metavanadates including VO_5 or VO_6 units. This may indicate that the geometries of the VO_4 tetrahedra for α-$Sr(VO_3)_2$ and $Ba(VO_3)_2$ are similar to those of the monovalent metal metavanadates. Finally, it is noted that correlations between the isotropic chemical shifts and structural parameters or the vanadium coordination state cannot immediately be derived. For the orthovanadates, δ_{iso} ranges from -420 to -791 ppm,[26] while, for the divalent metal metavanadates, it ranges from -468 to -658 ppm. Furthermore, differences in δ_{iso} of 50−60 ppm are observed for the two crystallographic ^{51}V sites of $Ca(VO_3)_2 \cdot 4H_2O$, $Pb(VO_3)_2$, $Ba(VO_3)_2$, and α-$Sr(VO_3)_2$ (cf. Table 1). These appear to be quite large differences, considering that the environments for the V^{5+} sites in these metavanadates are rather similar. Thus, we expect that further insight into the relationship between δ_{iso} (or the CSA tensors) and structure will require either models which consider the first and further distant coordination spheres of the V^{5+} ions or theoretical calculations of the electronic structure surrounding the V^{5+} ions. The experimental ^{51}V shielding data determined in this work form a suitable basis for such investigations, since precise values for δ_{iso} (and for δ_σ and η_σ) have been obtained.

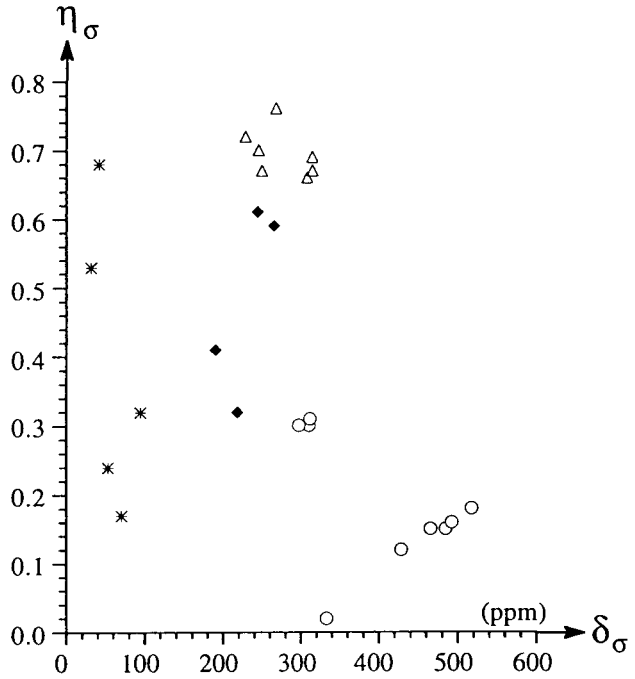

Figure 10. Graph illustrating the ^{51}V CSA asymmetry parameter (η_σ) as function of the shielding anisotropy (δ_σ) for orthovanadates (asterisks), monovalent metal metavanadates (triangles), and divalent metal metavanadates including VO_5 or VO_6 units (circles) and VO_4 tetrahedra (diamonds). The CSA parameters are taken from Table 1 for the divalent metal metavanadates and from ref 26 for the orthovanadates and monovalent metal metavanadates.

Conclusions

Magnitudes and relative orientations of ^{51}V quadrupole coupling and chemical shielding tensors have been obtained for a series of divalent metal metavanadates from ^{51}V MAS NMR spectra of the central and satellite transitions. Thereby, improved characterization of these vanadates has been achieved, since earlier ^{51}V NMR studies focused only on a determination of the chemical shielding parameters. Furthermore, the precision of the NMR parameters has been improved by employing a high magnetic field (14.1 T), which enhances the effects from the chemical shielding anisotropy. The brannerite type metavanadates possess quadrupole coupling constants that are among the strongest observed so far for vanadates and which result in the observation of partly resolved second-order quadrupolar line shapes for the spinning sidebands even at 14.1 T. The optimized NMR data show strong similarities in these parameters for the isostructural groups of divalent metal metavanadates, which allows different types of metavanadates to be distinguished and characterized on the basis of their anisotropic NMR parameters. For example, the similarities in NMR data for $Ba(VO_3)_2$ and α-$Sr(VO_3)_2$ strongly suggest that α-$Sr(VO_3)_2$ (of unknown crystal structure) is isostructural with $Ba(VO_3)_2$ (i.e., orthorhombic, *C*222). Linear correlations between the experimental ^{51}V quadrupole coupling tensor elements and estimates of the electric field gradient tensors from point-monopole calculations have been observed and found useful in the assignment of the ^{51}V quadrupole couplings for the metavanadates containing two

crystallographically different ^{51}V sites. Comparison of the chemical shielding data for the divalent metal metavanadates with those reported for orthovanadates and monovalent metavanadates shows that these parameters can be used to distinguish the different types of ^{51}V environments in vanadates. Furthermore, we expect that an improved insight into the relationships between the NMR data and parameters characterizing the local ^{51}V environments may be gained from models which also include the quadrupole coupling parameters and the isotropic chemical shifts. Especially the latter parameters may yield significant structural information since they varies by 190 ppm for the studied metavanadates.

Acknowledgment. The use of the facilities at the Instrument Centre for Solid-State NMR Spectroscopy, University of Aarhus, sponsored by the Danish Research Councils (SNF and STVF), Teknologistyrelsen, Carlsbergfondet, and Direktør Ib Henriksens Fond, is acknowledged.

IC991243Z